Unified Understanding of Nonlinear Rheology near the Jamming Transition Point

Takeshi Kawasaki and Kunimasa Miyazaki
Department of Physics, Nagoya University, Nagoya 464-8602, Japan

(Received 1 December 2023; accepted 9 May 2024; published 25 June 2024)

When slowly sheared, jammed packings respond elastically before yielding. This linear elastic regime becomes progressively narrower as the jamming transition point is approached, and rich nonlinear rheologies such as shear softening and hardening or melting emerge. However, the physical mechanism of these nonlinear rheologies remains elusive. To clarify this, we numerically study jammed packings of athermal frictionless soft particles under quasistatic shear γ. We find the universal scaling behavior for the ratio of the shear stress σ and the pressure P, independent of the preparation protocol of the initial configurations. In particular, we reveal shear softening $\sigma/P \sim \gamma^{1/2}$ over an unprecedentedly wide range of strain up to the yielding point, which a simple scaling argument can rationalize.

DOI: 10.1103/PhysRevLett.132.268201

Introduction.—A disordered packing of grains becomes a solid when its density, or the packing fraction φ, exceeds the jamming transition density φ_J [1]. Critical behaviors are observed in the vicinity of φ_J, which is established both theoretically [2,3] and experimentally [4]. Examples include the nontrivial but universal criticality of the contact number, pressure, elastic moduli, and non-Debye vibrational properties at low frequencies, to name a few [2,3,5,6]. However, these behaviors are established for undeformed systems.

The jamming criticality of the mechanical response under deformation, or the nonlinear rheology, is far less understood than the undeformed counterparts. The stationary nonlinear rheology under a constant strain-rate $\dot{\gamma}$ (and, thus, at large strain $\gamma \gg 1$) has been studied for decades, and the scaling law (typically for the viscosity η) is being actively updated [3,7–14]. The transient nonlinear rheology at a finite γ in the quasistatic limit is as rich as the stationary rheology, but this regime remains largely unexplored even in frictionless grains. Jammed packing responds elastically if the strain γ is small and yields and becomes plastic if γ exceeds the yielding point γ_y. Recent numerical studies revealed diverse mechanical properties between elastic and plastic regimes. The linear elastic window becomes progressively narrow as $\varphi \to \varphi_J$ from the above and completely disappears at the transition point, whereas yielding point γ_y is insensitive to the distance from φ_J. As the system is deformed beyond the elastic window, it first experiences the "shear softening," where stress is proportional to $\gamma^{1/2}$ [15–20]. This shear softening is universally observed near φ_J right next to the elastic regime. When strained further, the stress increases sharply. This is called shear hardening, and it persists until the system eventually yields [21]. A similar sudden increase of the stress is observed even below φ_J, where the system originally in a stress-free unjammed phase acquires the rigidity beyond a finite strain, which is called shear jamming [21–24]. Though the shear jamming was originally thought to occur only in frictional particle systems [25,26], it is observed also in frictionless particles if the systems are exposed to mechanical training [22,27] or thermal annealing [23,28–35]. The shear hardening in trained packing should be contrasted with the shear *melting*, observed in untrained packings, which are fragile against deformation [36–38]. These diverse rheologies imply that they sensitively depend on the preparation protocols of the packings, such as training and annealing. Significant dependence of nonlinear rheology on the training and annealing has been reported for a wide range of amorphous solids [39–43]. However, the unified understanding of these complex rheologies remains elusive.

In this Letter, we disentangle the shear melting, jamming or hardening, and softening by numerically investigating the two- and three-dimensional jammed packings of frictionless soft particles under athermal quasistatic (AQS) shear strains γ for varieties of jammed packing. We recognize that φ_J varies depending on both the packing preparation protocol and, more importantly, the strain γ. We also show that the shear softening is the only essential mechanism at work, and σ/P is proportional to $\gamma^{1/2}$ between the onset of the softening at γ_s and the yielding point at γ_y. Our results lucidly demonstrate that stress and pressure undergo the shear melting or shear hardening because the jamming transition density φ_J progressively increases or decreases depending on the initial configurations as the system is deformed. Therefore, if the distance from φ_J is monitored to be fixed (or if one observes the ratio of the stress to pressure), one can eliminate the effects of hardening and melting. We also provide a simple scaling argument that rationalizes the numerical results.

Numerical modeling.—The systems we study are two- and three-dimensional (2D and 3D) equimolar binary mixtures of frictionless particles with diameters σ_L and σ_S. The size ratio of small and large particles is $\sigma_L/\sigma_S = 1.4$. The interaction potential between the jth and kth particles is given by

$$U(r_{jk}) = \frac{\epsilon}{\alpha}\{1 - (r_{jk}/\sigma_{jk})\}^{\alpha}\Theta(\sigma_{jk} - r_{jk}), \qquad (1)$$

where $r_{jk} = |\mathbf{r}_j - \mathbf{r}_k|$, $\sigma_{jk} = (\sigma_j + \sigma_k)/2$, and $\Theta(x)$ is the Heaviside step function [44]. Here σ_j is the diameter of the jth particle. In our simulations, we use σ_S, ϵ, and ϵ/σ_S^2 as units of length, energy, and stress (pressure), respectively. The particle number is $N = 1156$ and the power in the potential is $\alpha = 2.0$ (harmonic potential) unless otherwise stated. To confirm that the finite size effect does not affect the conclusions, we performed simulations in the range $N = 288$ to 16 384 in 2D harmonic potential (see Figs. S1, S2 in the Supplemental Material [45]). We also perform simulations of 3D harmonic or 2D Hertzian potential systems ($\alpha = 2.5$), which show qualitatively the same results as 2D harmonic systems, as shown in Figs. S6 and S7 in Supplemental Material [45]. The particles are driven to a quasistatic state using the FIRE algorithm [46,47] for energy minimization. We also apply shear stabilization to remove residual stress for the initial configurations [36] (see Ref. [45]).

We consider a configuration quasistatic when the average force amplitude acting on a particle is less than $10^{-14}\epsilon/\sigma_S$. This threshold value is determined by the numerical accuracy of double-precision numbers plus round-off errors. We perform constant volume simulations for most parts of the main text, except for the data of $\varphi_J(\gamma)$ shown in Fig. 3, obtained from constant pressure simulations. Figures S3–S9 in Supplemental Material [45] present the stress-strain curves and other relevant results with constant pressure simulations.

Results.—We generated the initial configurations through mechanical training by a quasistatic compression-decompression cycle with various amplitudes, or "depths" [22,28]. Depth here is defined as the maximum density φ_{MAX} to which the system is compressed during the cycle. The mechanical training stabilizes the jammed configurations. Figure 1(a) presents the potential energy per particle $U = (1/N)\sum_{j>k} U(r_{jk})$ as a function of φ during the cycle. We first prepare a random configuration with $\varphi \lesssim 0.84$ and increase φ by $\Delta\varphi = 10^{-4}$ each steps up to φ_{MAX}. Then we decrease φ by $\Delta\varphi = 10^{-4}$ each step if $U > 10^{-8}$ and $\Delta\varphi = 10^{-6}$ otherwise. We define the initial jamming transition density, φ_{J0}, as the point where U becomes $U < 10^{-16}$ for the first time. Figure 1(b) shows φ_{J0} as a function of φ_{MAX}. We observe that as φ_{MAX} increases, φ_{J0} also increases when φ_{MAX} is less than 1.2; when φ_{MAX} is greater than 1.2, φ_{J0} slightly decreases and then converges to $\varphi_{J0} \approx 0.846$. This indicates that an optimal training amplitude may exist at which the system is most efficiently packed at the bottom of the geometric landscape, leading to the largest φ_J. Similar optimal amplitudes have been observed in sheared systems [43,48]. We only consider the mechanically trained initial configuration. We believe other protocols, such as thermal annealing, will have similar effects [21,34]. In the present study, once the jamming transition point is reached, the packing fraction is gradually changed toward the target φ to obtain the initial configuration for the mechanical response.

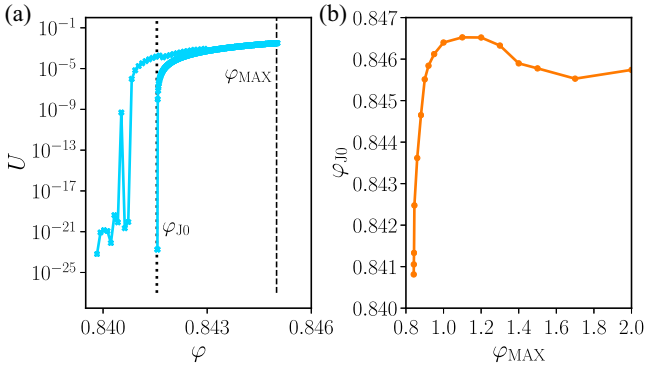

FIG. 1. (a) Preparation protocol for initial configurations: φ dependence of potential energy per particle U during the compression-decompression process. φ_{MAX} is the maximum packing fraction during this process, and φ_{J0} is the packing fraction when $U < 10^{-16}$ for the first time during decompression. (b) Jamming transition density, φ_{J0} as a function of the depth of the mechanical training, φ_{MAX}.

Next, we investigate the mechanical response of thus-obtained initial configurations to quasistatic steady shear [49], using the Lees-Edwards boundary conditions [50]. A small affine shear strain $\Delta\gamma(n)$ is applied to drive the particles in each step. Then, the positions of the particles are relaxed to the equilibrium position using the FIRE algorithm to minimize the energy. The shear strain evolves as $\gamma(n+1) = \gamma(n) + \Delta\gamma(n)$. When the accumulated shear strain is in the regime $\gamma < 10^{-3}$, $\Delta\gamma(n)$ is logarithmically increased from 10^{-7} (or 10^{-9}) to 10^{-3}; when $\gamma > 10^{-3}$, $\Delta\gamma(n)$ is fixed to 10^{-3}. The shear stress and the pressure are measured using a quasistatic steady shear configuration. The stress tensor is defined as $\sigma_{\alpha\beta} = (1/L^2)\sum_{j>k}(r_{jk}^{\alpha} r_{jk}^{\beta}/r_{jk})(\partial U/\partial r_{jk})$, where $\alpha, \beta \in \{x, y\}$, $r_{jk}^{x} = x_{jk}$ and $r_{jk}^{y} = y_{jk}$ [50]. The shear stress is given by the off-diagonal components of the stress tensor, σ_{xy} or σ_{yx}. The pressure is computed from the diagonal components, $P = -(\sigma_{xx} + \sigma_{yy})/2$. We consider the mechanical response to quasistatic shear of the initial configurations that are mechanically trained with different φ_{MAX}. All data shown below are averaged over at least 15 independent runs (typically, more than 100).

Figure 2 shows the mechanical response with respect to γ for various $\delta\varphi(= \varphi - \varphi_{J0})$ at $\varphi_{MAX} = 1.2$. Figure 2(a) is the γ dependence of the shear stress $\sigma_{xy}(\gamma)$, or the stress-strain curves. Slightly above the jamming transition, $\delta\varphi \gtrsim 0$, the stress-strain curve exhibits a unique behavior as the shear strain increases. For small γ, we observe an elastic response $\sigma_{xy} = G\gamma$, where G is the shear modulus. After the elastic regime, the system enters the shear-softening regime where $\sigma_{xy} \sim \gamma^{1/2}$. A shear hardening is

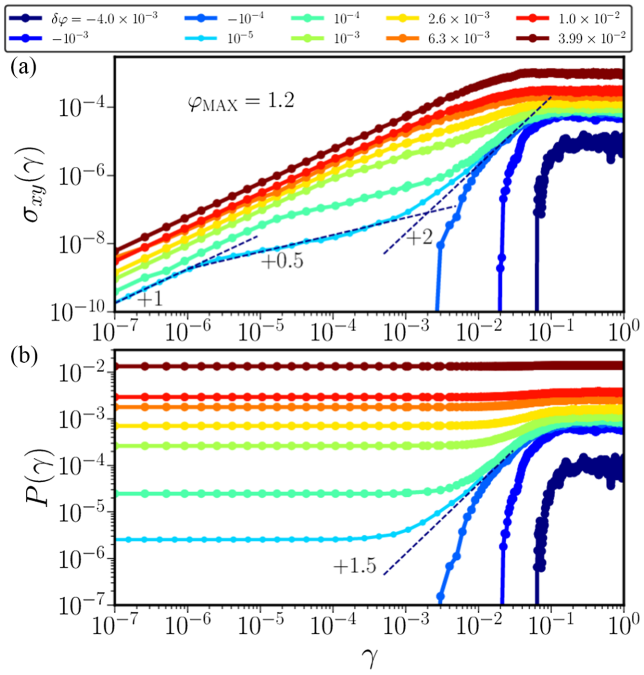

FIG. 2. Constant volume mechanical response to strain γ for various $\delta\varphi(=\varphi-\varphi_{\mathrm{J0}})$. Initial configurations are prepared with $\varphi_{\mathrm{MAX}} = 1.2$, where $\varphi_{\mathrm{J0}} \sim 0.8465$. (a) σ_{xy} vs γ. The dashed lines represent $\sigma_{xy} \propto \gamma$, $\sigma_{xy} \propto \gamma^{0.5}$, and $\sigma_{xy} \propto \gamma^{2.0}$, respectively. (b) P vs γ. The dashed line represents $P \propto \gamma^{1.5}$.

observed at larger γ, where the stress increases sharply as $\sigma_{xy} \sim \gamma^2$. The system eventually yields at even larger γ, where σ_{xy} becomes almost constant. The yielding point $\gamma_{\mathrm{y}} \simeq 5\times10^{-2}$ is insensitive to the densities. When the initial configuration is in the unjammed phase, or $\delta\varphi \lesssim 0$, the system undergoes the shear jamming behavior; $\sigma_{xy}(\gamma)$ is 0 (unjammed) at small γ's, but it abruptly jumps to a finite value before the system enters the hardening regime $\sigma_{xy}(\gamma) \sim \gamma^2$ at intermediate γ's. We also focus on the γ dependence of the pressure $P(\gamma)$, which will provide important insight for our understanding of the nonlinear mechanical response [as in Fig. 2(b)]. When $\delta\varphi > 0$, as γ is increased, P remains almost constant through both elastic and softening regimes, but it sharply increases as $P \sim \gamma^{1.5}$ in the shear hardening regime. Note that in the hardening regime, the power law exponents for $P(\gamma)$ differ from that of $\sigma_{xy}(\gamma) \sim \gamma^2$ by 0.5.

We summarize the pressure-strain curves in Fig. 2(b) as the jamming phase diagram for a wide range of φ and shear strain γ (see the color map of Fig. 3). We observe that, when $\varphi \gtrsim \varphi_{\mathrm{J0}}$, the system is always jammed and P is finite. When $\varphi \lesssim \varphi_{\mathrm{J0}}$, on the other hand, $P = 0$ at small γ's but becomes nonzero, and the system shear jams at $\gamma \sim 10^{-2}$, that is observed as the sharp boundary in the color map. The shear jamming is not observed if $\varphi \lesssim 0.842$, however large the strain is. This color map clearly demonstrates the fluid and jammed phases are demarcated by the sharp jamming

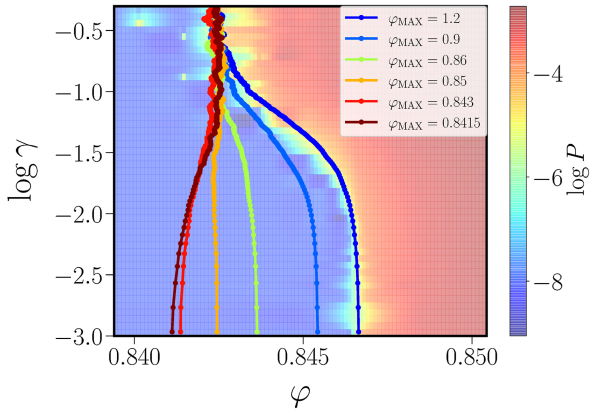

FIG. 3. P as a function of γ and φ at $\varphi_{\mathrm{MAX}} = 1.2$ by integrating constant volume simulation data as shown in Fig. 2(b). (Plotted points overlaid on the color map) φ dependence of γ obtained under constant pressure at $P = 10^{-6}$ representing as $\varphi_{\mathrm{J}}(\gamma)$ for various φ_{MAX}.

transition line $\varphi_{\mathrm{J}}(\gamma)$, which is an S-shaped continuous function of γ.

So far, we focused on the well-trained system with relatively large φ_{MAX} (= 1.2), for which φ_{J0} is conceivably large compared with that of the untrained system. Henceforth, we study how the jamming transition line $\varphi_{\mathrm{J}}(\gamma)$ varies with the initial jamming transition density φ_{J0}, which can be tuned by varying φ_{MAX}. This is key to understanding the complicated mechanical responses observed above. To compute $\varphi_{\mathrm{J}}(\gamma)$, we switch to the constant pressure simulation under steady shear [23] (see Supplemental Material [45]). Superimposed on the color map in Fig. 3 discussed above is the γ dependence of the volume fraction obtained at small but finite pressure at $P = 10^{-6}$. As P is infinitesimally small, the measured volume fraction is interpreted as the jamming transition point $\varphi_{\mathrm{J}}(\gamma)$. Different lines correspond to the simulation for initial packings obtained for different φ_{MAX}'s. $\varphi_{\mathrm{J}}(\gamma)$ in the small γ limit is φ_{J0} shown in Fig. 1(b). $\varphi_{\mathrm{J}}(\gamma)$'s starting from different φ_{J0}'s are constant at small γ but start bending around $\gamma \approx 10^{-2}$, and eventually converge to a common density $\varphi_{\mathrm{J}\infty} \approx 0.843$ at large γ (due to the loss of the memory imprinted in the initial configurations [22,35,51]). The convergence occurs at $\gamma \gtrsim 0.1$, slightly above the yielding point γ_{y}. $\varphi_{\mathrm{J}\infty}$ agrees with the jamming transition point estimated from stationary nonlinear rheology under a constant $\dot{\gamma}$ [11,35,49,52–55]. Note that φ_{J0}'s obtained for small φ_{MAX}'s (< 0.86) are smaller than $\varphi_{\mathrm{J}\infty}$ [53,55,56]. When these poorly trained jammed packings slightly above φ_{J0} are strained, the density crosses $\varphi_{\mathrm{J}}(\gamma)$ at a finite γ and undergoes the shear melting (see Fig. S4 in Supplemental Material [45]).

Inspired by the fact that in constant-volume simulations, both σ_{xy} and P show the shear jamming and shear hardening, we plot the ratio of the stress to the pressure, or the friction coefficient $\mu = \sigma_{xy}/P$ in Fig. 4(a). We use the same

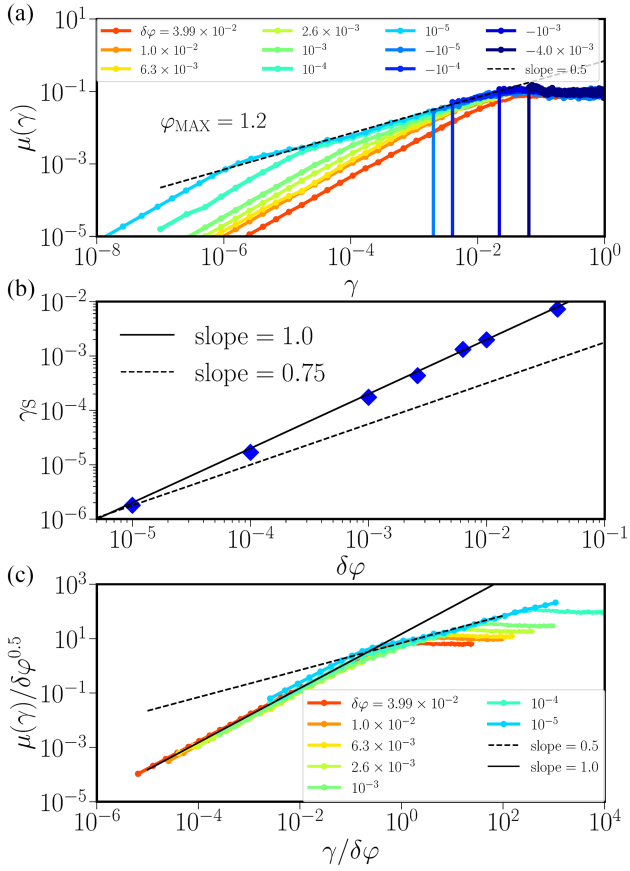

FIG. 4. Constant volume nonlinear rheology with initial configurations trained at $\varphi_{\mathrm{MAX}} = 1.2$. (a) Friction coefficient $\mu(\gamma) = \sigma_{xy}(\gamma)/P(\gamma)$ vs γ for various $\delta\varphi = \varphi - \varphi_{\mathrm{J0}}$. (b) The crossover shear strain γ_{S} between the elastic and softening regimes as a function of $\delta\varphi = \varphi - \varphi_{\mathrm{J0}}$, found to follow $\gamma_{\mathrm{S}} \sim \delta\varphi$. (c) $\mu(\gamma)/\delta\varphi^{0.5}$ vs $\gamma/\delta\varphi$ for the data shown in (a), where $\delta\varphi = \varphi - \varphi_{\mathrm{J0}}$.

data of Fig. 2 at $\varphi_{\mathrm{MAX}} = 1.2$ for various $\delta\varphi = \varphi - \varphi_{\mathrm{J0}}$ for both below and above the transition point. The result uncovers surprisingly simple and novel rheology. Between the elastic regime at small γ where $\mu \propto \gamma$ and the yielding regime at large γ where both σ_{xy} and P are independent of γ, there lies a wide range of the softening regime where $\mu \propto \gamma^{0.5}$. No shear jamming or hardening is observed in μ. The shear jamming or hardening is apparent when looking at σ_{xy} and P in the constant volume simulations. This is due to the progressive change of the jamming transition density as the strain is increased. We address that μ is independent of $\delta\varphi$ in the softening regime, indicating that the softening is the critical behavior. One reads two messages in Fig. 4(a). First, the shear-softening persists over an unprecedentedly wide range. It is observed even for originally unjammed packings ($\varphi < \varphi_{\mathrm{J0}}$) exactly when the system crosses $\varphi_{\mathrm{J}}(\gamma)$ and acquires the rigidity at the shear-hardening point (see the discontinuous change of μ for $\delta\varphi < 0$ in the figure). Second, the data reveal that the shear softening alone dictates the critical behavior above and below the jamming transition point. The fact that shear jamming or hardening originates from the continuous increase of $\varphi - \varphi_{\mathrm{J}}(\gamma)$ with γ implies that σ_{xy} at the constant pressure should show the same behavior as $\mu(\gamma)$ since the distance from the jamming transition point is always kept constant if P is fixed. This is the case, as shown in Figs. S3, S5–S9, in Supplemental Material [45].

As Fig. 4(a) clearly demarcates the elastic and softening regimes, we estimate the onset strain of the softening, γ_{S}. We find $\gamma_{\mathrm{S}} \sim (\varphi - \varphi_{\mathrm{J0}})^x$ with $x = 1$, as shown in Fig. 4(b), consistent with the values reported in the literature [16,18,19]. A different scaling exponent $x = 3/4$ was reported [17] which was derived from a scaling argument [57]. We will discuss the discrepancies in the exponents later. The origin of the scaling of the onset strain is purely geometrical. The softening sets in when the particles are displaced by an overlap distance to exchange the excess contacts proportional to $\delta\varphi$. We verify that the cage-relative displacement of the particle (i.e., the relative displacement) [58,59] is proportional to the γ, and softening occurs where this exceeds the overlap length, as shown in Fig. S9 in Supplemental Material [45]. Here we also find that the yielding point γ_{y} is insensitive to $\delta\varphi$ because the corresponding particle displacement is equivalent to the cage size, which is always $\mathcal{O}(0.1)$ regardless of the overlap length.

Lastly, let us explain the observed softening behaviors using a simple scaling argument in the softening regime. The prerequisites are a scaling ansatz $\sigma_{xy} \sim P^a\gamma^b$, and our observations that $\gamma_{\mathrm{s}} \propto \delta\varphi$. First, from the fact that γ_{y} is insensitive to $\delta\varphi$ and σ_{xy} is proportional to P beyond γ_{y} [see Fig. 4(a)], thus $\sigma_{xy} \sim P^a 1^b \sim P$ and then we readily obtain $a = 1$. Second, in the opposite limit at γ_{s}, σ_{xy} should be converged to $P\gamma_{\mathrm{s}}^b \sim \delta\varphi^{\alpha-1}\delta\varphi^b$, where $P \sim \delta\varphi^{\alpha-1}$ [2,3,5]. For the stress to match at the elastic region $\sigma_{xy} = G\gamma_{\mathrm{s}} \sim \delta\varphi^{\alpha-1/2}$, we arrive at $b = 1/2$. Here we used $G \sim \delta\varphi^{\alpha-3/2}$ [2,3,5,60]. From this argument, we finally obtain a deceptively simple scaling law for $\mu(\gamma) = \sigma_{xy}(\gamma)/P(\gamma)$ as,

$$\mu(\gamma) = \delta\varphi^{1/2}\mathcal{F}(\gamma/\delta\varphi), \tag{2}$$

where $\mathcal{F}(x) = x (x \ll 1)$ and $\mathcal{F}(x) = x^{1/2}$ (otherwise). We emphasize that φ_{J} used in $\delta\varphi = \varphi - \varphi_{\mathrm{J}}$ is a function of γ, *not* the initial jamming density φ_{J0} at $\gamma = 0$.

The above scaling argument dissolves the controversy over the different exponents $x = 1$ and $3/4$ for the onset strain γ_{s} [17,57]. $x = 3/4$ originates from the scaling argument for the energy under shear $E(\gamma) = E_0 + G\gamma^2$. Using the scaling for the energy $E_0 \propto \delta\varphi^\alpha$ and modulus $G \propto \delta\varphi^{\alpha-3/2}$, we obtain $E \sim \delta\varphi^\alpha\{1 + (\gamma/\delta\varphi^{3/4})^2\}$. This expression implies that the crossover strain γ_{s} is scaled as $\delta\varphi^{3/4}$. However, the shear modulus is assumed to be independent of γ in this argument. As we demonstrated in

this Letter, the elastic-softening crossover takes place at $\gamma_s \sim \delta\varphi$ *before* γ reaches $\delta\varphi^{3/4}$.

Summary.—In this Letter, we resolved the mechanism of nonlinear rheology observed near the jamming transition by systematically tuning the stability of the initial jamming configuration by mechanical training [22,28,61]. This allows us to explore a wide range of jamming density φ_{J0} from the very fragile packing at low φ_{J0} to the stable packing at high φ_{J0}. We numerically found that complex nonlinear mechanical responses such as melting, shear jamming, and hardening can be explained solely by the distance from the jamming transition points, which varies continuously with strain. They can be all scaled out, and the emerging scaling picture is simple and robust; only the softening prevails between the linear elastic and the yielding regime. We also find the softening region over the unprecedently wide range of γ. The next natural question is the interplay of the softening $\sigma_{xy}(\gamma) \sim \gamma^{1/2}$ and the critical viscoelastic scaling $\sigma_{xy}(\omega) \sim \omega^{1/2}$ [62]. Both algebraic scalings share the same exponent, and they both claim a criticality where $\delta\varphi$ is scaled out as the jamming transition point is approached from above. We have already demonstrated that the stress shows the softening behavior even below jamming, i.e., $\varphi < \varphi_J$, but only if the strain rate is finite. In other words, $\sigma_{xy} \propto \dot{\gamma}^{1/2} = (\omega\gamma)^{1/2}$, a result implying the scaling for $\sigma_{xy}(\omega, \gamma)$ [42].

We thank S. Sastry, H. Hayakawa, M. Otsuki, Y. Jin, H. Yoshino, A. Zaccone, M. K. Nandi, H. Bessho, and S. Tomioka for their valuable discussions. This work was supported by the JST FOREST Program (JPMJFR212T), AMED Moonshot Program (JP22zf0127009), and JSPS KAKENHI (24H02203, 23H04503, 22H04472, 20H05157, 20H00128).

[1] A. J. Liu and S. R. Nagel, Nonlinear dynamics: Jamming is not just cool any more, Nature (London) **396**, 21 (1998).
[2] C. S. O'Hern, L. E. Silbert, A. J. Liu, and S. R. Nagel, Jamming at zero temperature and zero applied stress: The epitome of disorder, Phys. Rev. E **68**, 011306 (2003).
[3] M. van Hecke, Jamming of soft particles: Geometry, mechanics, scaling and isostaticity, J. Phys. Condens. Matter **22**, 033101 (2010).
[4] T. S. Majmudar, M. Sperl, S. Luding, and R. P. Behringer, Jamming transition in granular systems, Phys. Rev. Lett. **98**, 058001 (2007).
[5] C. S. O'Hern, S. A. Langer, A. J. Liu, and S. R. Nagel, Random packings of frictionless particles, Phys. Rev. Lett. **88**, 075507 (2002).
[6] H. A. Makse, N. Gland, D. L. Johnson, and L. M. Schwartz, Why effective medium theory fails in granular materials, Phys. Rev. Lett. **83**, 5070 (1999).
[7] J. Paredes, M. A. J. Michels, and D. Bonn, Rheology across the Zero-temperature jamming transition, Phys. Rev. Lett. **111**, 015701 (2013).
[8] P. Olsson and S. Teitel, Critical scaling of shear viscosity at the jamming transition, Phys. Rev. Lett. **99**, 178001 (2007).
[9] M. Otsuki and H. Hayakawa, Critical behaviors of sheared frictionless granular materials near the jamming transition, Phys. Rev. E **80**, 011308 (2009).
[10] T. Kawasaki, D. Coslovich, A. Ikeda, and L. Berthier, Diverging viscosity and soft granular rheology in non-Brownian suspensions, Phys. Rev. E **91**, 012203 (2015).
[11] D. Vågberg, P. Olsson, and S. Teitel, Critical scaling of Bagnold rheology at the jamming transition of frictionless two-dimensional disks, Phys. Rev. E **93**, 052902 (2016).
[12] P. Olsson, Dimensionality and viscosity exponent in shear-driven jamming, Phys. Rev. Lett. **122**, 108003 (2019).
[13] A. Ikeda, T. Kawasaki, L. Berthier, K. Saitoh, and T. Hatano, Universal relaxation dynamics of sphere packings below jamming, Phys. Rev. Lett. **124**, 058001 (2020).
[14] K. Saitoh, T. Hatano, A. Ikeda, and B. P. Tighe, Stress relaxation above and below the jamming transition, Phys. Rev. Lett. **124**, 118001 (2020).
[15] C. Coulais, A. Seguin, and O. Dauchot, Shear modulus and dilatancy softening in granular packings above jamming, Phys. Rev. Lett. **113**, 198001 (2014).
[16] M. Otsuki and H. Hayakawa, Avalanche contribution to shear modulus of granular materials, Phys. Rev. E **90**, 042202 (2014).
[17] D. Nakayama, H. Yoshino, and F. Zamponi, Protocol-dependent shear modulus of amorphous solids, J. Stat. Mech. (2016) 104001.
[18] J. Boschan, D. Vågberg, E. Somfai, and B. P. Tighe, Beyond linear elasticity: Jammed solids at finite shear strain and rate, Soft Matter **12**, 5450 (2016).
[19] S. Dagois-Bohy, E. Somfai, B. P. Tighe, and M. van Hecke, Softening and yielding of soft glassy materials, Soft Matter **13**, 9036 (2017).
[20] J. Boschan, S. Luding, and B. P. Tighe, Jamming and irreversibility, Granular Matter **21**, 58 (2019).
[21] D. Pan, F. Meng, and Y. Jin, Shear hardening in frictionless amorphous solids near the jamming transition, PNAS Nexus **2**, pgad047 (2023).
[22] N. Kumar and S. Luding, Memory of jamming–multiscale models for soft and granular matter, Granular Matter **18**, 58 (2016).
[23] V. Babu, D. Pan, Y. Jin, B. Chakraborty, and S. Sastry, Dilatancy, shear jamming, and a generalized jamming phase diagram of frictionless sphere packings, Soft Matter **17**, 3121 (2021).
[24] D. Pan, Y. Wang, H. Yoshino, J. Zhang, and Y. Jin, A review on shear jamming, Phys. Rep. **1038**, 1 (2023).
[25] D. Bi, J. Zhang, B. Chakraborty, and R. P. Behringer, Jamming by shear, Nature (London) **480**, 355 (2011).
[26] R. P. Behringer and B. Chakraborty, The physics of jamming for granular materials: A review, Rep. Prog. Phys. **82**, 012601 (2018).
[27] H. A. Vinutha and S. Sastry, Disentangling the role of structure and friction in shear jamming, Nat. Phys. **12**, 578 (2016).
[28] P. Chaudhuri, L. Berthier, and S. Sastry, Jamming transitions in amorphous packings of frictionless spheres occur

over a continuous range of volume fractions, Phys. Rev. Lett. **104**, 165701 (2010).
[29] M. Ozawa, T. Kuroiwa, A. Ikeda, and K. Miyazaki, Jamming transition and inherent structures of hard spheres and disks, Phys. Rev. Lett. **109**, 205701 (2012).
[30] M. Ozawa, L. Berthier, and D. Coslovich, Exploring the jamming transition over a wide range of critical densities, SciPost Phys. **3**, 027 (2017).
[31] P. Urbani and F. Zamponi, Shear yielding and shear jamming of dense hard sphere glasses, Phys. Rev. Lett. **118**, 038001 (2017).
[32] Y. Jin, P. Urbani, F. Zamponi, and H. Yoshino, A stability-reversibility map unifies elasticity, plasticity, yielding, and jamming in hard sphere glasses, Sci. Adv. **4**, eaat6387 (2018).
[33] V. Babu and S. Sastry, Criticality and marginal stability of the shear jamming transition of frictionless soft spheres, Phys. Rev. E **105**, L042901 (2022).
[34] Y. Jin and H. Yoshino, A jamming plane of sphere packings, Proc. Natl. Acad. Sci. U.S.A. **118**, e2021794118 (2021).
[35] D. Vågberg, P. Olsson, and S. Teitel, Glassiness, rigidity, and jamming of frictionless soft core disks, Phys. Rev. E **83**, 031307 (2011).
[36] S. Dagois-Bohy, B. P. Tighe, J. Simon, S. Henkes, and M. van Hecke, Soft-sphere packings at finite pressure but unstable to shear, Phys. Rev. Lett. **109**, 095703 (2012).
[37] C. P. Goodrich, S. Dagois-Bohy, B. P. Tighe, M. van Hecke, A. J. Liu, and S. R. Nagel, Jamming in finite systems: Stability, anisotropy, fluctuations, and scaling, Phys. Rev. E **90**, 022138 (2014).
[38] K. VanderWerf, A. Boromand, M. D. Shattuck, and C. S. O'Hern, Pressure dependent shear response of jammed packings of frictionless spherical particles, Phys. Rev. Lett. **124**, 038004 (2020).
[39] M. Ozawa, L. Berthier, G. Biroli, A. Rosso, and G. Tarjus, Random critical point separates brittle and ductile yielding transitions in amorphous materials, Proc. Natl. Acad. Sci. U.S.A. **115**, 6656 (2018).
[40] P. Leishangthem, A. D. S. Parmar, and S. Sastry, The yielding transition in amorphous solids under oscillatory shear deformation, Nat. Commun. **8**, 14653 (2017).
[41] T. Kawasaki and L. Berthier, Macroscopic yielding in jammed solids is accompanied by a nonequilibrium first-order transition in particle trajectories, Phys. Rev. E **94**, 022615 (2016).
[42] K. Nagasawa, K. Miyazaki, and T. Kawasaki, Classification of the reversible–irreversible transitions in particle trajectories across the jamming transition point, Soft Matter **15**, 7557 (2019).
[43] W.-T. Yeh, M. Ozawa, K. Miyazaki, T. Kawasaki, and L. Berthier, Glass stability changes the nature of yielding under oscillatory shear, Phys. Rev. Lett. **124**, 225502 (2020).
[44] D. J. Durian, Foam mechanics at the bubble scale, Phys. Rev. Lett. **75**, 4780 (1995).
[45] See Supplemental Material at http://link.aps.org/supplemental/10.1103/PhysRevLett.132.268201 for additional information on simulation algorithms, dimensionality, potential, system size and ensemble dependencies, and the relationship between microscopic particle dynamics and mechanical properties.
[46] F. Shuang, P. Xiao, R. Shi, F. Ke, and Y. Bai, Influence of integration formulations on the performance of the fast inertial relaxation engine (FIRE) method, Comput. Mater. Sci. **156**, 135 (2019).
[47] E. Bitzek, P. Koskinen, F. Gähler, M. Moseler, and P. Gumbsch, Structural relaxation made simple, Phys. Rev. Lett. **97**, 170201 (2006).
[48] P. Das, H. A. Vinutha, and S. Sastry, Unified phase diagram of reversible–irreversible, jamming, and yielding transitions in cyclically sheared soft-sphere packings, Proc. Natl. Acad. Sci. U.S.A. **117**, 10203 (2020).
[49] C. Heussinger and J.-L. Barrat, Jamming transition as probed by quasistatic shear flow, Phys. Rev. Lett. **102**, 218303 (2009).
[50] M. P. Allen and D. J. Tildesley, *Computer Simulation of Liquids* (Oxford University Press, New York, 1988).
[51] N. C. Keim, J. D. Paulsen, Z. Zeravcic, S. Sastry, and S. R. Nagel, Memory formation in matter, Rev. Mod. Phys. **91**, 035002 (2019).
[52] E. Lerner, G. Düring, and M. Wyart, A unified framework for non-Brownian suspension flows and soft amorphous solids, Proc. Natl. Acad. Sci. U.S.A. **109**, 4798 (2012).
[53] W. Zheng, S. Zhang, and N. Xu, Jamming of packings of frictionless particles with and without shear, Chin. Phys. B **27**, 066102 (2018).
[54] D. Vågberg, D. Valdez-Balderas, M. A. Moore, P. Olsson, and S. Teitel, Finite-size scaling at the jamming transition: Corrections to scaling and the correlation-length critical exponent, Phys. Rev. E **83**, 030303(R) (2011).
[55] A. Peshkov and S. Teitel, Comparison of compression versus shearing near jamming, for a simple model of athermal frictionless disks in suspension, Phys. Rev. E **107**, 014901 (2023).
[56] A. Peshkov and S. Teitel, Critical scaling of compression-driven jamming of athermal frictionless spheres in suspension, Phys. Rev. E **103**, L040901 (2021).
[57] C. P. Goodrich, A. J. Liu, and J. P. Sethna, Scaling ansatz for the jamming transition, Proc. Natl. Acad. Sci. U.S.A. **113**, 9745 (2016).
[58] H. Shiba, Y. Yamada, T. Kawasaki, and K. Kim, Unveiling dimensionality dependence of glassy dynamics: 2D infinite fluctuation eclipses inherent structural relaxation, Phys. Rev. Lett. **117**, 245701 (2016).
[59] B. Illing, S. Fritschi, H. Kaiser, C. L. Klix, G. Maret, and P. Keim, Mermin-Wagner fluctuations in 2D amorphous solids, Proc. Natl. Acad. Sci. U.S.A. **114**, 1856 (2017).
[60] A. Zaccone and E. Scossa-Romano, Approximate analytical description of the nonaffine response of amorphous solids, Phys. Rev. B **83**, 184205 (2011).
[61] H. Matsuyama, M. Toyoda, T. Kurahashi, A. Ikeda, T. Kawasaki, and K. Miyazaki, Geometrical properties of mechanically annealed systems near the jamming transition, Eur. Phys. J. E **44**, 133 (2021).
[62] B. P. Tighe, Relaxations and rheology near jamming, Phys. Rev. Lett. **107**, 158303 (2011).